SIMULATION OF FREE-SURFACE VISCOUS FLOWS BY A FINITE-ELEMENT FRONT-TRACKING APPROACH

L. Charlot[1], A. Hay[2], S. Etienne[3] and D. Pelletier[4]

Département de Génie Mécanique,
Ecole Polytechnique de Montréal,
Montréal, Québec, Canada.

1 Introduction

Water waves and their effects on floating or submerged bodies is an important area of research in engineering. It covers a wide spectrum of applications presenting significant difficulties and challenges to understand and predict. Investigation is further compounded by the fact that laboratory experiments on scaled prototype are difficult and expensive. Furthermore, scaling laboratory results from model to full scale configuration is not always possible. On the other hand, Computational Fluid Dynamics is complementary to experiments because it provides a large amount of detailed data on flows. Consequently the predictive capability and scientific analysis must rely partly on computational models.
One of the main issues in the numerical modeling of free-surface flows is that the location of the free surface is part of the solution of the problem. In *front-capturing* approaches, the free surface is captured on a fixed mesh, like in the Volume Of Fluid or level-set methods. An alternative consists in following the free surface with the deformable mesh (*i.e. front-tracking* methods). The former approaches lead to a more general simulation procedure because interfaces can undergo arbitrary changes of topology; as an example it allows for the simulation of breaking waves. However, the latter provides a more accurate methodology because the location of the free surface is explicitly known and not subjected to smearing from numerical diffusion.
In the present work, we use a *front-tracking boundary fitted methodology* to model free-surface flows. In this approach, the free-surface matches one of the boundaries of the computational domain and follows its deformations in time while resulting grid motions are accounted for by an Arbitrary Lagrangian Eulerian (ALE) approach. Interior domain deformation is obtained by using the pseudo-solid method which generates domain displacements through quasi-static linear elasticity equations. The pseudo-solid approach is very general and allows for efficiently treating complex geometries. To avoid robustness and stability issues which lead to excessively long simulation times or algorithm breakdown, we develop a fully coupled implicit procedure with highly stable time integrators.

2 Modeling and numerical approach

We consider the laminar incompressible unsteady Navier-Stokes equations on the domain Ω_α as illustrated in Fig. 1. Furthermore, we consider free-surface flows for which moving interfaces must be simulated. For air/water free-surface flows, the air can be neglected and only the water needs to be simulated so that the interface can be modeled as one of the boundary of the domain. Using a front-tracking approach, the free-surface matches one of the boundaries of the

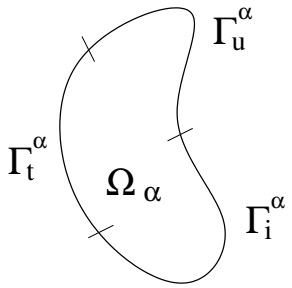

Figure 1: Fluid domain including a free-surface

computational domain ($\Gamma_{\boldsymbol{i}}^\alpha$ in Fig. 1) and follows its deformations in time while grid motions are accounted for by an ALE

[1] *lise.charlot@polymtl.ca*, *Ph.D.* student
[2] *alexander.hay@polymtl.ca*, Research associate
[3] *stephane.etienne@polymtl.ca*, Assistant professor
[4] *dominique.pelletier@polymtl.ca*, Full professor and presenting author

approach. Following the ALE methodology, the velocity of the moving reference frame $\boldsymbol{v_m}$ is introduced and equations are expressed in the ALE coordinate system:

$$\nabla \cdot \boldsymbol{u} = 0, \tag{1}$$

$$\rho \frac{\partial \boldsymbol{u}}{\partial t} + \rho((\boldsymbol{u} - \boldsymbol{v_m}) \cdot \nabla)\boldsymbol{u} = -\nabla p + \nabla \cdot \boldsymbol{\tau}(\boldsymbol{u}) + \boldsymbol{f}, \tag{2}$$

where $\boldsymbol{\tau}(\boldsymbol{u})$ is the viscous fluid stress which for Newtonian fluids is given by:

$$\boldsymbol{\tau}(\boldsymbol{u}) = \mu \left(\nabla \boldsymbol{u} + \nabla^T \boldsymbol{u} \right).$$

As illustrated in Fig. 1, the fluid domain boundary is divided into three parts $\Gamma^\alpha = \Gamma^\alpha_{\boldsymbol{u}} \cup \Gamma^\alpha_{\boldsymbol{t}} \cup \Gamma^\alpha_{\boldsymbol{i}}$ which all depend on α. Dirichlet conditions are prescribed on $\Gamma^\alpha_{\boldsymbol{u}}$, Neumann conditions on $\Gamma^\alpha_{\boldsymbol{t}}$ and free-surface conditions hold on $\Gamma^\alpha_{\boldsymbol{i}}$:

$$\boldsymbol{u} = \overline{\boldsymbol{u}} \quad \text{on } \Gamma^\alpha_{\boldsymbol{u}}, \tag{3}$$

$$\boldsymbol{\sigma} \cdot \boldsymbol{n} = -p\boldsymbol{n} + \boldsymbol{\tau}(\boldsymbol{u}) \cdot \boldsymbol{n} = \overline{\boldsymbol{t_f}} \quad \text{on } \Gamma^\alpha_{\boldsymbol{t}}, \tag{4}$$

$$(\boldsymbol{u} - \boldsymbol{v_m}) \cdot \boldsymbol{n} = 0 \quad \text{on } \Gamma^\alpha_{\boldsymbol{i}}, \tag{5}$$

$$\boldsymbol{\sigma} \cdot \boldsymbol{n} = \boldsymbol{0} \quad \text{on } \Gamma^\alpha_{\boldsymbol{i}}, \tag{6}$$

where $\overline{\boldsymbol{u}}$ and $\overline{\boldsymbol{t_f}}$ are the prescribed values of the boundary velocity and traction respectively. The kinematic condition Eq. (5) states that the air/water interface is a material surface while the dynamic condition Eq. (6) expresses the continuity of normal stresses (without phase change and neglecting surface tension effects). Given that the air is neglected, no forces act on the free-surface.

In the front-tracking methodology, we need to account for domain deformation due to the motion of the boundary $\Gamma^\alpha_{\boldsymbol{i}}$. We choose the pseudo-solid approach [1] which generates the domain deformation through quasi-static linear elasticity equations:

$$\nabla \cdot \left(\frac{1}{2} \lambda_{ps} tr \left(\nabla \boldsymbol{\chi} + \nabla^T \boldsymbol{\chi} \right) \boldsymbol{I} + \mu_{ps} \left(\nabla \boldsymbol{\chi} + \nabla^T \boldsymbol{\chi} \right) \right) = 0, \tag{7}$$

where λ_{ps} and μ_{ps} are the Lamé coefficients of the pseudo-solid. $\boldsymbol{\chi}$ is subjected to homogeneous Dirichlet condition everywhere on the domain boundary except at the free-surface where $\boldsymbol{\chi}$ is constrained to follow the interface motion. In the present work, we use the pseudo-solid displacement to define the velocity of the moving reference frame for the ALE methodology: $\boldsymbol{v_m} = \frac{\partial \boldsymbol{\chi}}{\partial t}$. Note that special attention must be paid when evaluating $\boldsymbol{v_m}$ and its divergence from $\boldsymbol{\chi}(t)$ to satisfy the so-called Geometric Conservation Law in the ALE formulation in order to preserve the order of accuracy of time integrators. The interested reader is referred to [2] for details.
In 2D, the free-surface boundary conditions Eqs. (5-6) result in 3 conditions for the components of the fluid velocity $\boldsymbol{u} = [u, v]^T$ and the pseudo-solid displacement $\boldsymbol{\chi} = [\chi, \eta]^T$. Hence, one condition is missing given that there is no physical information to govern the tangential displacement of points onto the free-surface. One is thus free to arbitrarily choose an additional condition as part of the pseudo-solid model. In the discrete setting, we choose to set that the ratio of boundary segment lengths on each side of a boundary point is preserved through the free-surface deformation. This additional condition guarantees smooth mesh deformation at the free-surface.

The flow equations are solved by a finite element method using either the $P_2 - P_1$ Taylor-Hood element (third-order accuracy for the velocity and second-order accuracy for the pressure) or the $P_1 - P_1$ element (second-order accuracy for velocity and pressure). The resulting system of non-linear algebraic equations are linearized by Newton's method and solved using a sparse direct solver. Time integration is performed by the 1st (referred to as RK11 in what follows), 3rd (RK32) and 5th (RK53) order Radau IIA schemes. These implicit Runge-Kutta schemes are 1st, 3rd and 5th order time-accurate for velocity and 1st, 2nd and 3rd order time-accurate for the pressure (see [2]). For details on their implementation in the framework of free-surface flows using the ALE formulation, the interested reader is referred to [3].

3 Numerical results

We present several applications using the numerical methodology presented previously. In this abstract, we only provide limited descriptions of the cases and results while more details will be given during the presentation.

3.1 Sloshing in tanks

We first consider the large amplitude sloshing in a tank as described in [4]. For this case, the free surface is at rest at the initial time and we use slip boundary conditions on walls. The tank is submitted to a horizontal displacement following $A(1-\cos(\omega t))$ with $\omega = 1.5$ corresponding to resonance condition as detailed in [4]. Figure 2 shows the free surface elevation on the right wall of the tank with time for the RK11 and RK32 time-stepping schemes and several time steps given as a fraction of the period of the sloshing. As can be seen, time step convergence is easily achieved by the higher order accurate RK32 time integration scheme even for large time steps while RK11 (*i.e.* the implicit backward Euler method) would require excessively small time steps to reach convergence. It shows that the use of high-order time stepping schemes constitutes a much more efficient numerical procedure (even though one time step is computationally more demanding and expensive).

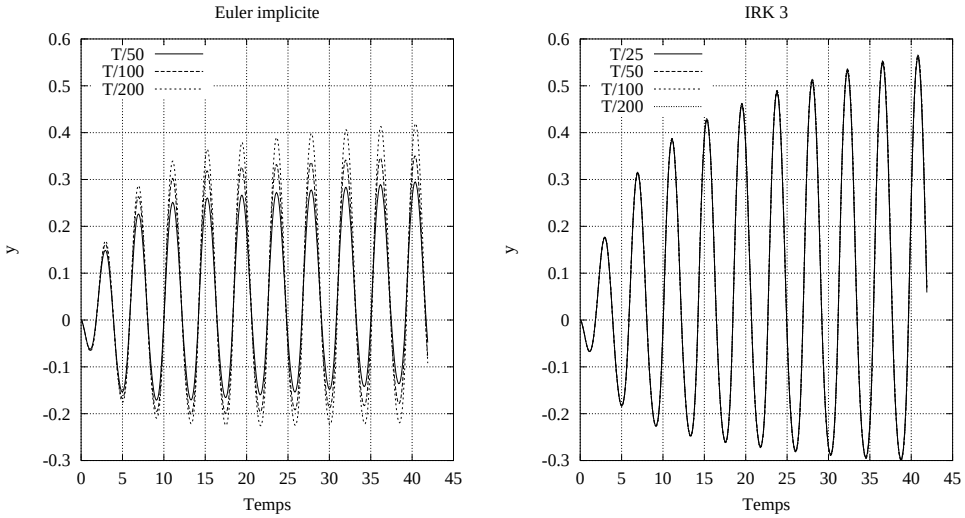

(a) RK11 (b) RK32

Figure 2: Free surface elevation on the right wall of the tank with time.

We also consider the sloshing test case described in [5] which provides a comparison with different methods based on [6]. In this setting, the free surface is deformed at the initial time following $70. + 12.[1. - (x/53.)^2] \exp^{(x/76.)^2}$ and latter evolves freely under gravity. The present numerical results are confronted to those reported in [5] in Table 1. As can be seen, the agreement is quite good on the average.

	min	average	max	present
free surface elevation	-3.860	-3.796	-3.720	-3.797
streamwise velocity	-2.480	-2.410	-2.280	-2.415
crossflow velocity	-0.690	-0.547	-0.363	-0.571

Table 1: Velocity and free surface elevation at $x = 60m$ and $t = 9, 2s$.

3.2 Wave propagation in a canal

This case is also described thoroughly in [5]. It corresponds to the propagation of a solitary wave in a long canal. For the present numerical simulation, we use the $P_1 - P_1$ element and the RK32 time stepping scheme. The analytically generated wave does not perfectly match a real water wave so that some free surface oscillations are observed behind the wave. We compare our results to those in [5] in figure 3(a). As can been seen, the resulting oscillations are similar in amplitude and shape. Figure 3(b) shows the free surface elevation along the canal every 10 seconds. After $20s$ of simulation the wave is properly developed and has an amplitude of $0.097m$. The amplitude latter slightly decreases with time to reach $0.093m$ at time $t = 120s$ due to viscous dissipation.

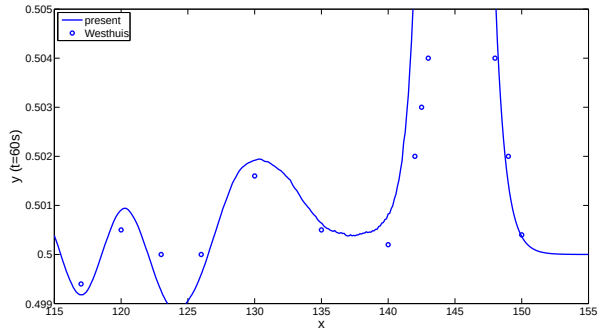

(a) Oscillations behind the wave at time $t = 60s$

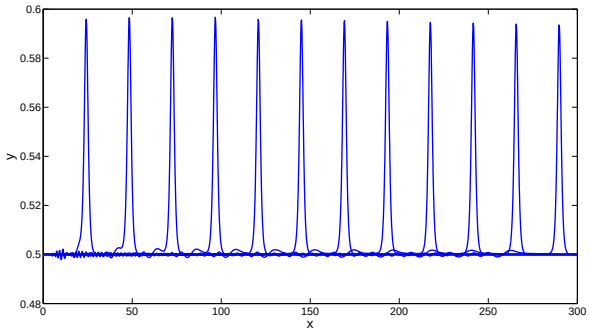

(b) Free surface elevation every 10 s

Figure 3: Wave propagation in a canal.

3.3 Flow over a submerged cylinder

We now numerically reproduce the experimental set-up of Chaplin [7] who measured the forces experienced by a submerged horizontal cylinder with its axis parallel to the crests in deep-water waves. In our setting, waves are generated by a wave-making machine located at the far left of the domain which is modeled by the left boundary oscillating horizontally according to $A\sin(\omega t)$ with $A = 0.1D$. Figure 4 shows the loads on the cylinder and free-surface elevation (with and without, referred to as *sans*, the cylinder) at time $t = 188s$ for a cylinder submerged at a distance $d = 1.5D$ below the free surface at rest.

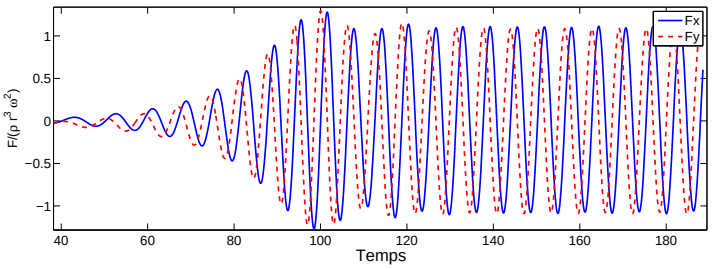

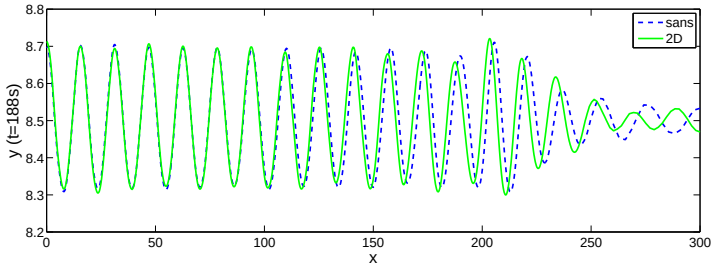

Figure 4: Loads on the cylinder (left) and free-surface elevation (right) at time $t = 188s$ for $d = 1.5D$.

References

[1] P. A. Sackinger, P.R. Schunk, and R. R. Rao. A newton-raphson pseudo-solid domain mapping technique for free and moving boundary problems:a finite element implementation. *Journal of Computational Physics*, 125:83–103, 1996.

[2] S. Etienne, A. Garon, and D. Pelletier. Perspective on the geometric conservation law and finite element methods for ALE simulations of incompressible flow. *J. of Comput. Phys.*, 228:2313–2333, 2009.

[3] L. Charlot, S. Etienne, and D. Pelletier. Verification of a free surface adaptive finite element solution algorithm. In *49th AIAA Aerospace Sciences Meeting including The New Horizons Forum and Aerospace Exposition*, Orlando, Florida, January 2011. AIAA-2011-666.

[4] W. Dettmer and D. Peric. A computational framework for free surface fluid flows accounting for surface tension. *Computer Methods in Applied Mechanics and Engineering*, 195:3028–3071, 2006.

[5] J.-H. Westhuis. *The numerical simulation of nonlinear waves in a hydrodynamic model test basin*. PhD thesis, Universiteit Twente, The Netherlands, 2001.

[6] A. Nestegård. Comparative study of fully non-linear wave simulation programs. Technical report, Det Norske Veritas, 1994. Det Norske Veritas, Technical Report 94-2041.

[7] J. R. Chaplin. Nonlinear forces on a horizontal cylinder beneath waves. *Journal of Fluid Mechanics*, 147:449–464, 1984.